ChemPubSoc Europe

DOI: 10.1002/slct.201600166

Chemistry SELECT Communications

Biological Chemistry & Chemical Biology

In situ Detection of a Single Bacterium in Complex Environment by Hyperspectral CARS Imaging**

Weili Hong,[a] Chien-Sheng Liao,[a] Hansen Zhao,[d] Waleed Younis,[c] Yinxin Zhang,[a, e] Mohamed N. Seleem,*[c] and Ji-Xin Cheng*[a, b]

Detection of bacteria is essential for clinical diagnosis of infectious disease and food safety purposes. However, it is still a challenging task to rapidly detect bacteria, especially in their natural environment. By fiber-laser based hyperspectral coherent anti-Stokes Raman scattering (CARS) imaging, we showed that bacteria can be detected in a single cell level using spectral focusing in the C–H stretching region, with a total recording time of 1-2 minutes. With phase retrieval and multivariate curve resolution analysis, we further showed that a single bacterium can be detected in complex environment such as milk and urine, without need of culturing, labelling, or sample contact. Our work promises hyperspectral CARS imaging to be a mobile and inexpensive setup for *in situ* detection of bacteria and bacterial activity studies.

Rapid detection and analysis of bacteria in their natural environment are critical to the clinical diagnosis of infectious diseases[1] and food safety purposes.[2] Current methods, including bright field optical microscopy, gram staining, and motility testing, require long bacterial culture times, lack accuracy due to limited information, and are not sensitive in complex environments.[3]

Newly developed molecular techniques based on the sequence analysis of the ribosomal DNA (rDNA) or ribosomal RNA (rRNA) of bacteria have facilitated rapid and sensitive detection of bacteria. As a nucleic acid amplification method, polymerase chain reaction (PCR) has been used to detect bacteria in low concentrations. PCR is useful for detection of bacteria that are hard to culture. However, this technique is time consuming,[4] suffers from contamination,[5] and does not provide enough information about the number and spatial localization of bacteria. Fluorescent in situ hybridization (FISH) with rRNA-targeted probes is another molecular technique for detection of a single bacterium with spatial localization capacity.[6] However, this technique depends on the availability of suitable discriminate probes.[7] Notably, both techniques are destructive to bacterial cells.

Linear vibrational spectroscopy has shown great potential for label-free bacteria detection. Fourier-transform infrared (FTIR)[8] and Raman spectroscopy have proven effective for rapid identification of bacteria.[3,7,9,10] These techniques use vibrational spectra as a 'fingerprint' signature for bacteria identification, allowing culture-free, rapid, and non-destructive detection.[10] However, these techniques also have their limitations. For example, FTIR suffers from strong water absorbance[11] and Raman spectroscopy produces very weak signals and therefore requires long acquisition time. The acquisition time to get one Raman spectrum in an area of 1 μm^2 for a single bacterium is 60–90 seconds.[7] Thus, it takes 6–9 hours to scan an area of 60×60 μm^2 in order to get the spatial distribution information. By increasing the signal level, surface enhanced Raman spectroscopy (SERS)[12] has also been used for bacteria identification.[13] However, SERS requires direct contact of the sample with the substrate, which is not suitable for *in situ* detection of bacteria.

Coherent anti-Stokes Raman scattering (CARS) microscopy is a label-free technique that offers dramatic improvement in signal levels over spontaneous Raman microscopy.[14] In most CARS imaging experiments, a pump-probe beam (ω_p) and a Stokes beam (ω_s) are used to generate an anti-Stokes field through interaction with the specimen. When the beating frequency (ω_p-ω_s) matches the frequency of a molecule vibration, a resonance occurs, resulting in a peak in the CARS spectrum. The CARS signal is accompanied by a non-resonant background,[15] and two phase retrieval methods have been developed to extract the Raman signal.[16,17] Hyperspectral CARS, which records a stack of images that contain a spectrum at each pixel, has been used for noninvasive detection of single bacterial endospores.[18]

Here, we report a compact, fiber-laser based hyperspectral CARS microscope for *in situ* detection of a single living bacte-

[a] *Dr. W. Hong, C.-S. Liao, Prof. Y. Zhang, Prof. J.-X. Cheng*
Weldon School of Biomedical Engineering, Purdue University
West Lafayette, Indiana 47907, USA
E-mail: jcheng@purdue.edu
[b] *Prof. J.-X. Cheng*
Department of Chemistry, Purdue University
West Lafayette, Indiana 47907, USA
[c] *Dr. W. Younis, Prof. M. N. Seleem*
Department of Comparative Pathobiology
Purdue College of Veterinary Medicine, Purdue University
West Lafayette, Indiana 47907, USA
E-mail: mseleem@purdue.edu
[d] *H. Zhao*
Department of Chemistry, Tsinghua University
Beijing 100084, China
[e] *Prof. Y. Zhang*
College of Precision Instrument and Opte-Electronics Engineering, Tianjin University
Tianjin 300072, China
[**] *This work was supported by Army Medical Research Acquisition grant 107391 to JXC.*

Supporting information for this article is available on the WWW under http://dx.doi.org/10.1002/slct.201600166

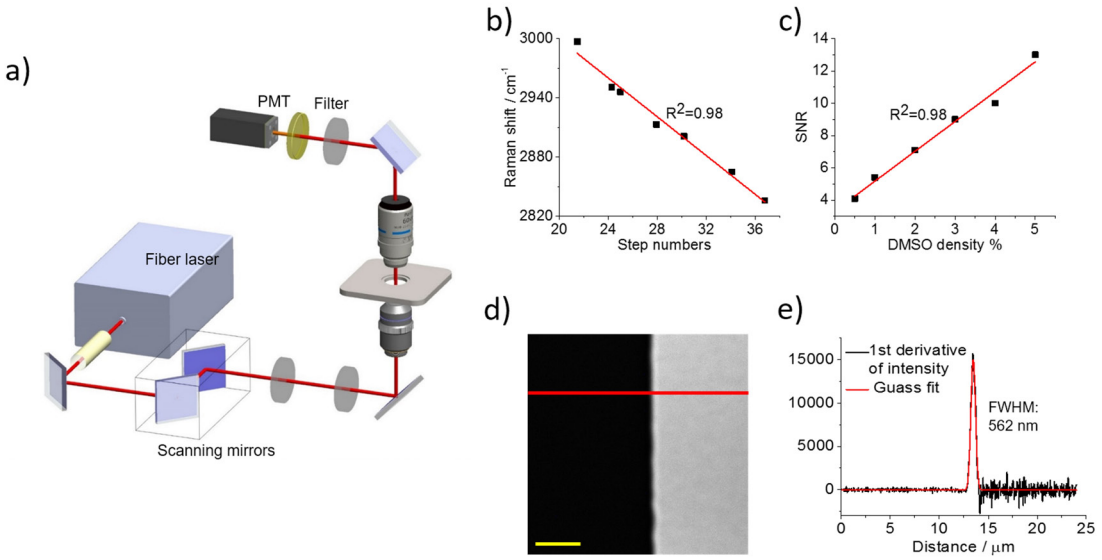

Figure 1. Schematic and performance of a fiber-laser based hyperspectral CARS imaging setup. a) Simplified schematic of the hyperspectral CARS microscope. The pump and Stokes beams were provided by a fiber laser system and were collinearly combined. The temporal delay stage between the pump and Stokes beams was inside the fiber laser box and controlled by a computer. PMT, photo-multiplier tube. b) Correlation of Raman shift with respect to the motor step numbers. The correlation was fitted by a linear curve ($R^2 = 0.98$). c) Detection sensitivity test using different concentrations of DMSO in water. The SNR was plotted against the DMSO concentration and fitted with a linear curve ($R^2 = 0.98$). d) CARS image of gold-glass edge. e) The first derivative plot of intensity over the gold-glass edge indicated by the red line in (c). The peak was fitted by a Gaussian distribution, and the full width at half maximum (FWHM) is 562 nm. Scale bars: 5 μm.

rium by its Raman signatures in the C–H vibration region. By phase retrieval and multivariate curve resolution (MCR) analysis, we show that a single *Escherichia coli* (*E. coli*) bacterium can be identified in a complex environment without need of culturing, labelling, or sample contact.

Figure 1**a** shows our fiber-laser based hyperspectral CARS microscope. A compact ultrafast fiber laser (FemtoFiber Dichro, TOPTICA Photonics) outputs two laser beams, one centered at 780 nm with ~10 nm bandwidth and ~80 mW average power, used as the pump beam, and the other centered at 1030 nm with ~10 nm bandwidth and ~250 mW average power, used as the Stokes beam. The laser power at the sample was ~24 mW for the pump beam, and ~75 mW for the Stokes beam. An optical delay stage was included in the fiber laser box, which allowed computer-control of the temporal delay between the pump and Stokes pulses. The two beams were collinearly combined, chirped by two 15 cm long SF57 glass rods for spectral focusing, and directed into a laser-scanning microscope. A 60X water immersion objective (UPLSAPO 60×W, OLYMPUS) with 1.20 numerical aperture focused the beams into the sample. An air condenser collected the light in the forward direction. Two filters (Z640/20x and D680/100 M, Chroma) blocked the pump and Stokes beams. The CARS photons were collected by a photo-multiplier tube (model H7422-40, Hamamatsu).

We first calibrated the Raman shift with respect to the pump-Stokes temporal overlap using Raman peaks of known chemicals. **Figure S1 a** shows the phase retrieved and normalized CARS spectra of cyclohexanone and methanol by adjusting the pump-Stokes temporal overlap. Corresponding spontaneous Raman spectra in the C–H stretching region from 2750 cm^{-1} to 3000 cm^{-1}, measured with a spectrograph (Shamrock SR-303i-A, Andor Technology) are shown in **Figure S1 b.** The CARS spectra were retrieved by a modified Kramers-Kronig method[16,19] and normalized by the glass non-resonant background which reflects the cross-correlation between the pump and Stokes pulses. Using the known Raman peaks shown in **Figure S1 b**, the translational stage positions in the fiber laser system were correlated to the Raman shifts by linear fitting ($R^2 = 0.98$), resulting in the calibration curve shown in Figure 1**b**. This curve allowed us to perform hyperspectral CARS imaging simply by scanning the optical delay stage.

We then evaluated the performance of the fiber-laser based hyperspectral CARS imaging setup in terms of detection sensitivity and spatial resolution. Dimethyl sulfoxide (DMSO) in an aqueous solution with different volume concentrations was used for the sensitivity test. **Figure S2** shows the representative phase-retrieved CARS images of different concentrations of DMSO-water mixture. The signal–to–noise ratio (SNR) of each image was correlated to the DMSO concentration by linear fitting, resulting in a linear correlation with $R^2 = 0.98$ (Figure 1**c**). The SNR for 0.5% DMSO was ~4, which is close to the detection limit of solid-laser based SRS microscopy.[20] We then estimated the spatial resolution using gold coated glass. Figure 1**d** shows the CARS image of the edge of gold coated glass, with the dark side being the gold coating, and the bright side being the glass. The intensity profile along the red line in Figure 1**d** was plotted, which shows the intensity change over the glass-gold interface. A clear peak, indicating the sharpness of the gold edge, was observed after first derivative of the intensity profiles over distance along the interface (Figure 1**e).**

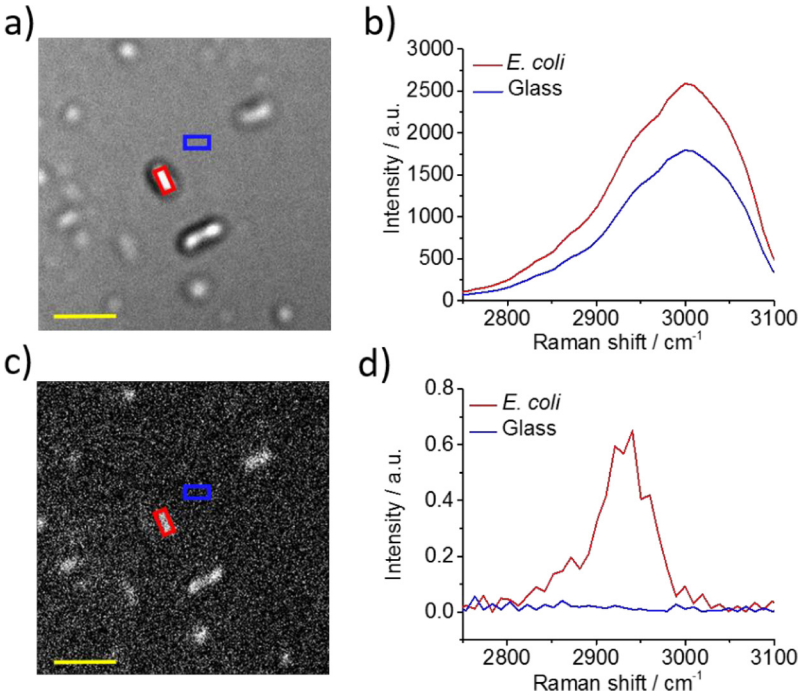

Figure 2. Detection of *E. coli* by hyperspectral CARS. a) Hyperspectral CARS image of air dried 10^3/ml concentrated *E. coli* on glass. b) Corresponding hyperspectral CARS profile of *E. coli* and the glass background. c) CARS image after phase retrieval. d) Corresponding phase-retrieved CARS spectrum of *E. coli* and the glass background. Scale bars: 5 μm.

The peak was fitted by a Gaussian distribution, and the spatial resolution was estimated to be ~ 562 nm, defined as the full width at half maximum (FWHM) of this peak. This spatial resolution is smaller than the diameter of most bacteria, which typically ranges from about 0.6 to 10 μm, indicating the capacity of our setup to quantitatively map individual bacterium.

To record the CARS spectra of a single living bacterium, we recorded a stack of 50 images of *E. coli* dispersed on a coverglass in the C–H stretching region from 2750 cm^{-1} to 3100 cm^{-1}, with a total recording time of 1-2 minutes. Figure 2**a** shows a 2930 cm^{-1} CARS image of 10^3/ml concentrated *E. coli* dried on a coverglass. Figure 2**b** shows the corresponding CARS spectra of a single *E. coli* bacterium and glass. The *E. coli* spectrum had a higher intensity than the glass spectrum, but the profiles of both *E. coli* and glass are similar. We considered the glass spectrum as the non-resonant background because glass does not have a vibrational Raman signal in the C–H stretching region. The *E. coli* spectrum contained both the Raman signal and the non-resonant background. We then applied phase retrieval to extract the signal from the background and obtained a Raman spectrum. Figure 2**c** shows the same area of Figure 2**a** after phase retrieval, and Figure 2**d** shows the corresponding spectra of *E. coli* and glass of Figure 2**b** after phase retrieval. After phase retrieval, the glass showed no Raman signal, and the retrieved Raman spectrum of a single *E. coli* bacterium showed a peak around 2930 cm^{-1}, which is in good agreement with the spontaneous Raman spectrum of *E. coli* shown in **Figure S3.**

To test whether water background affect the detection of bacteria, *E. coli* in water were examined. **Figure S4a** shows a 2930 cm^{-1} CARS image of *E. coli* fixed on a coverglass pre-coated with poly-l-lysine. **Figure S4b** shows the corresponding CARS spectra of a single *E. coli* bacterium and glass. After phase retrieval, the glass showed no Raman signal, and the retrieved Raman spectrum of *E. coli* in water is in good agreement with the retrieved Raman spectrum of dried *E. coli* (Figure 2**d**), indicating water background does not affect the detection of bacteria by hyperspectral CARS imaging.

We further examined whether a single *E. coli* bacterium in complex environment can be detected. We first applied our hyperspectral CARS imaging setup to map 10^8/ml concentrated *E. coli* mixed with non-homogenized milk and dried on a coverglass. Figure 3**a** shows a 2920 cm^{-1} CARS image of *E. coli*-milk mixture, with the corresponding spectra of *E. coli*, milk and glass shown in **Figure S6a.** The retrieved Raman spectrum (**Figure S6b**) of glass showed no peak; the retrieved Raman spectrum of *E. coli* showed a peak around 2930 cm^{-1}, arising from the C-H_3 stretching mode; the retrieved Raman spectrum of milk showed two peaks, at 2930 cm^{-1} and 2850 cm^{-1}, arising from the C-H_2 stretching mode, indicating abundant lipid components in milk. The hyperspectral CARS image stack of the *E. coli*-milk mixture was further analyzed by MCR[21] to reconstruct the quantitative concentration maps of *E. coli*, milk and the glass background. Figure 3**b** shows the overlapped concentration map of *E. coli* (red), milk (green) and glass background (gray). The red dashed rectangular in **Figures 3a** and **3b** shows a region where both *E. coli* and milk are present, the magnified image of this region is shown in **Figure S5.** In the single-frequency CARS image (Figure 3**a** and **Figure S5a**), *E. coli* is buried in milk lipid particle. By hyperspectral CARS combined with MCR analysis, *E. coli* was identified and clearly separated from the milk lipid particle (Figure 3**b** and **Figure S5b**). The spectra of *E. coli*, milk, and glass in **Figure S6a** were used as the input for three-component MCR analysis. Corresponding output spectra of *E. coli* and milk after phase retrieval are shown in Figure 3**c**. Pure milk dried on a coverglass was used as a control.

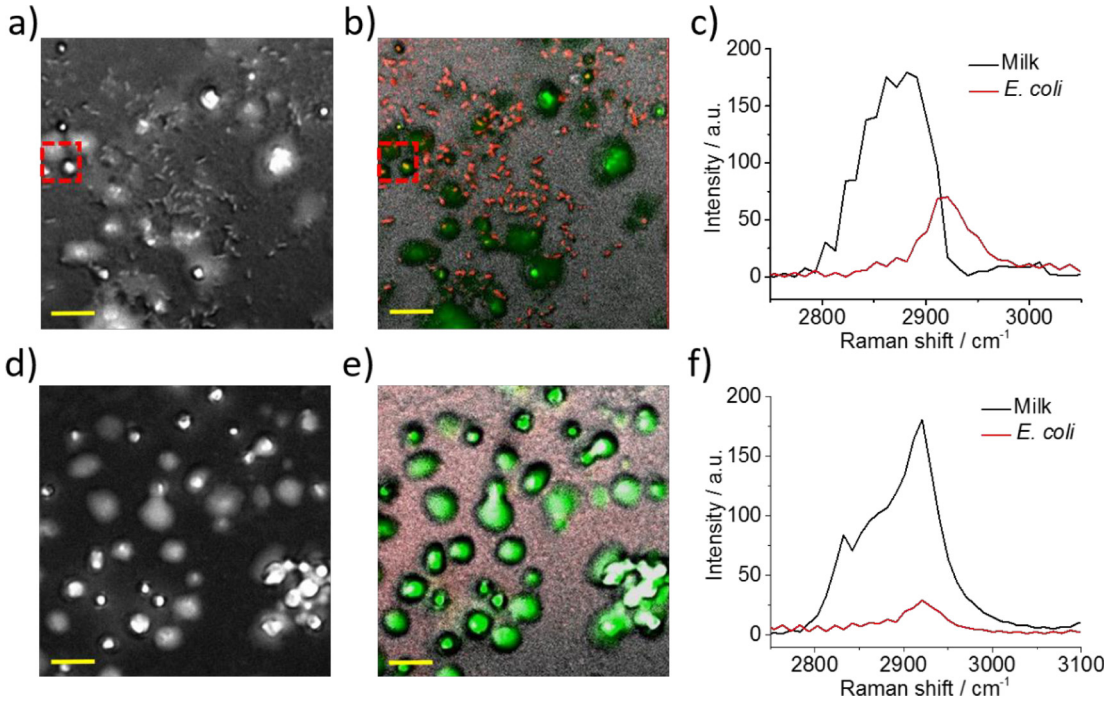

Figure 3. Detection of bacteria in milk. a) CARS image of *E. coli*-milk mixture. b) Reconstructed map of *E. coli* and milk components after MCR analysis. The *E. coli* is mapped with red color and the milk is mapped with green color. The red dashed rectangular in (a) and (b) indicate the location where *E. coli* and milk are overlapped. c) Corresponding phase retrieved output spectra of each component after MCR analysis. d) CARS image of milk alone dried on glass. e) Reconstructed map of *E. coli* and milk components after MCR analysis. f) Corresponding phase retrieved output spectra of each component after MCR analysis. Scale bars: 10 μm.

Figure 3**d** shows a 2920 cm^{-1} CARS image of milk. We applied the same spectra of *E. coli*, milk, and glass as the input for three-component MCR analysis and plotted the concentration maps (Figure 3**e**). As expected, only milk and glass components were identified. The corresponding output spectra are shown in Figure 3**f**.

We then examined whether a single *E. coli* bacterium in urine can be detected. We applied our hyperspectral CARS imaging setup to map 10^8/ml concentrated *E. coli* mixed with urine and dried on a coverglass. Figure 4**a** shows a 2920 cm^{-1} CARS image of *E. coli*-urine mixture. The hyperspectral CARS image stack was further analyzed by MCR to reconstruct the concentration maps of *E. coli*, urine and glass background. Figure 4**b** shows the overlapped concentration maps of *E. coli* (red), urine (green) and glass background (gray). The spectra of *E. coli*, urine, and glass were used as the input for three-component MCR analysis. Corresponding output spectra of *E. coli* and urine after phase retrieval are shown in Figure 4**c**. Pure urine dried on a coverglass was used as a control. Figure 4**d** shows a 2920 cm^{-1} CARS image of urine. We applied the same spectra of *E. coli*, urine, and glass as the input for three-component MCR analysis and plotted the concentration map (Figure 4**e**). As expected, only urine and glass components were identified. The corresponding output spectra are shown in Figure 4**f**.

In summary, we have demonstrated a fiber-laser based hyperspectral CARS imaging system for rapid, *in situ* detection of a single *E. coli* bacterium. Aided with phase retrieval and MCR analysis, we further demonstrated that a single *E. coli* bacterium can be identified in complex environment. Fiber lasers are compact and cost effective compared to solid state lasers.[22] These advantages allow CARS microscope to be a mobile and inexpensive setup for wide clinical and environmental use. Although we focused on bacteria detection in this study, bacterial metabolic activity can be further studied by monitoring the spectral changes. Further studies promise to render CARS microscopy a powerful tool for *in situ* detection of bacteria and for determining bacterial response to antibiotics.

Supporting Information

Details about sample preparation, MCR analysis, and phase retrieval can be found in supporting information summary paragraph.

Keywords: Bacteria · Fiber laser · Stimulated Raman scattering imaging · Vibrational spectroscopy

[1] R. Goodacre, R. Burton, N. Kaderbhai, A. M. Woodward, D. B. Kell, P. J. Rooney, *Microbiology* **1998**, *144*, 1157–1170.
[2] N. Moll, E. Pascal, D. H. Dinh, J.-P. Pillot, B. Bennetau, D. Rebiere, D. Moynet, Y. Mas, D. Mossalayi, J. Pistré, *Biosensors and Bioelectronics* **2007**, *22*, 2145–2150.
[3] K. Maquelin, L.-P. i. Choo-Smith, T. van Vreeswijk, H. P. Endtz, B. Smith, R. Bennett, H. A. Bruining, G. J. Puppels, *Analytical chemistry* **2000**, *72*, 12–19.

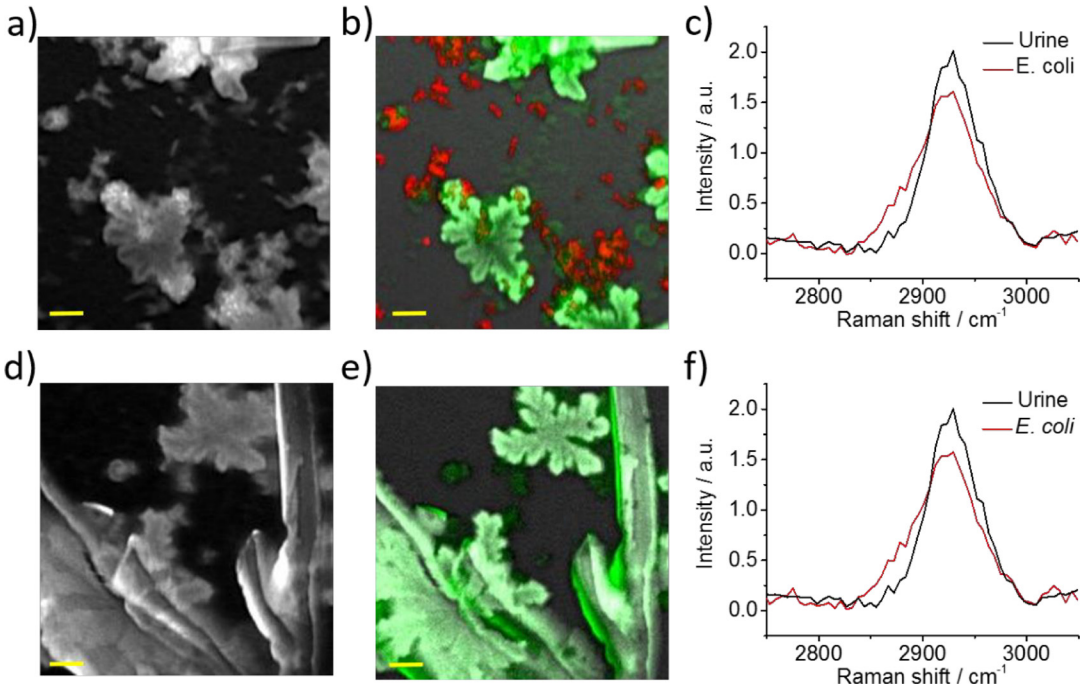

Figure 4. Detection of bacteria in urine. a) CARS image of *E. coli*-urine mixture. b) Reconstructed map of *E. coli* and urine components after MCR analysis. The *E. coli* is mapped with red color and the urine is mapped with green color. c) Corresponding phase retrieved output spectra of each component after MCR. d) CARS image of urine alone dried on a coverglass. e) Reconstructed map of *E. coli* and urine components after MCR analysis. f) Corresponding phase retrieved output spectra of each component after MCR. Scale bars: 10 μm.

[4] B. Currie, *Infect. Dis. Spec. Edn* **2011**, *14*; A. Lee, S. Mirrett, L. B. Reller, M. P. Weinstein, *Journal of clinical microbiology* **2007**, *45*, 3546–3548.
[5] E. Kastanos, A. Kyriakides, K. Hadjigeorgiou, C. Pitris, *International Journal of Spectroscopy* **2012**, *2012*.
[6] a) E. F. DeLong, G. S. Wickham, N. R. Pace, *Science* **1989**, *243*, 1360–1363; b) A. Moter, U. B. Göbel, *Journal of microbiological methods* **2000**, *41*, 85–112.
[7] W. E. Huang, R. I. Griffiths, I. P. Thompson, M. J. Bailey, A. S. Whiteley, *Analytical chemistry* **2004**, *76*, 4452–4458.
[8] D. Naumann, D. Helm, H. Labischinski, *Nature* **1991**, *351*, 81–82.
[9] a) A. Athamneh, R. Alajlouni, R. Wallace, M. Seleem, R. Senger, *Antimicrobial agents and chemotherapy* **2014**, *58*, 1302–1314; L. Mariey, J. Signolle, C. Amiel, J. Travert, *Vibrational Spectroscopy* **2001**, *26*, 151–159; b) R. Goodacre, B. Shann, R. J. Gilbert, E. M. Timmins, A. C. McGovern, B. K. Alsberg, D. B. Kell, N. A. Logan, *Analytical Chemistry* **2000**, *72*, 119–127; c) C. Xie, J. Mace, M. Dinno, Y. Li, W. Tang, R. Newton, P. Gemperline, *Analytical chemistry* **2005**, *77*, 4390–4397.
[10] K. Maquelin, C. Kirschner, L.-P. Choo-Smith, N. van den Braak, H. P. Endtz, D. Naumann, G. Puppels, *Journal of microbiological methods* **2002**, *51*, 255–271.
[11] S. Efrima, L. Zeiri, *Journal of Raman Spectroscopy* **2009**, *40*, 277–288.
[12] S. Nie, S. R. Emory, *science* **1997**, *275*, 1102–1106.
[13] a) R. M. Jarvis, R. Goodacre, *Analytical Chemistry* **2004**, *76*, 40–47; b) L. J. Goeller, M. R. Riley, *Applied spectroscopy* **2007**, *61*, 679–685.
[14] C. L. Evans, X. S. Xie, *Annu. Rev. Anal. Chem.* **2008**, *1*, 883–909.
[15] C. Zhang, D. Zhang, J.-X. Cheng, *Annual Review of Biomedical Engineering* **2015**, *17*.
[16] Y. Liu, Y. J. Lee, M. T. Cicerone, *Optics letters* **2009**, *34*, 1363–1365.
[17] E. M. Vartiainen, *JOSA B* **1992**, *9*, 1209–1214.
[18] a) G. I. Petrov, R. Arora, V. V. Yakovlev, X. Wang, A. V. Sokolov, M. O. Scully, *Proceedings of the National Academy of Sciences* **2007**, *104*, 7776–7779; b) D. Pestov, R. K. Murawski, G. O. Ariunbold, X. Wang, M. Zhi, A. V. Sokolov, V. A. Sautenkov, Y. V. Rostovtsev, A. Dogariu, Y. Huang, *Science* **2007**, *316*, 265–268; c) R. Arora, G. I. Petrov, V. V. Yakovlev, M. O. Scully, *Proceedings of the National Academy of Sciences* **2012**, *109*, 1151–1153.
[19] C. H. Camp, Y. J. Lee, M. T. Cicerone, *Journal of Raman Spectroscopy* **2015**.
[20] K. Wang, D. Zhang, K. Charan, M. N. Slipchenko, P. Wang, C. Xu, J. X. Cheng, *Journal of biophotonics* **2013**, *6*, 815–820.
[21] a) D. Zhang, P. Wang, M. N. Slipchenko, D. Ben-Amotz, A. M. Weiner, J.-X. Cheng, *Analytical chemistry* **2012**, *85*, 98–106; b) J. Jaumot, R. Gargallo, A. de Juan, R. Tauler, *Chemometrics and Intelligent Laboratory Systems* **2005**, *76*, 101–110.
[22] a) K. Kieu, B. G. Saar, G. R. Holtom, X. S. Xie, F. W. Wise, *Optics letters* **2009**, *34*, 2051–2053; H. Kano, H.-o. Hamaguchi, *Applied Physics Letters* **2005**, *86*, 121113; b) G. Krauss, T. Hanke, A. Sell, D. Träutlein, A. Leitenstorfer, R. Selm, M. Winterhalder, A. Zumbusch, *Optics letters* **2009**, *34*, 2847–2849.
[23] P. Wang, B. Liu, D. Zhang, M. Y. Belew, H. A. Tissenbaum, J. X. Cheng, *Angewandte Chemie International Edition* **2014**, *53*, 11787–11792.

Submitted: March 1, 2016
Accepted: March 1, 2016